

A Study on Fast Startup Simulation of the Soluble-Boron-Free SMR ATOM

Yunseok Jeong, Ahmed Amin E. Abdelhameed, and Yonghee Kim*
Korea Advanced Institute of Science and Technology (KAIST)
291 Daehak-ro, Yuseong-gu, Daejeon, Korea, 34141
*yongheekim@kaist.ac.kr

1. Introduction

The water-cooled small modular reactor (SMR) is being recognized as one of the next generation nuclear reactor concepts due to its enhanced passive safety and advanced design features.

Soluble-boron is actively used in commercial PWRs because it does not significantly distort local power distribution and it reduces the dependence on active control rod movements. However, it suffers from several disadvantages including slow reactivity response, near-zero moderator temperature coefficient (MTC) issue with a high soluble-boron concentration, etc., which hinders the flexible load-following operations of SMRs.

In the meantime, it has been shown that a soluble-boron-free (SBF) reactor design offers advantages for passively autonomous load-follow and frequency control operations. In addition, no complex de-boration facility and associated components are required, which improves the integrity of the system. With the comprehensive consideration of the aforementioned issues, an innovative soluble-boron-free SMR design named ATOM (Autonomous transportable on-demand reactor module) was proposed, which is characterized by a small excess reactivity during the entire irradiation period from BOC (beginning of cycle) to EOC (end of cycle). Several studies show that the ATOM has remarkable performance in terms of passive load-follow operations [1].

When designing a nuclear power plant, it is necessary and important to demonstrate that the reactor can be safely started and the power can be reliably increased from the hot-zero power to full power condition. In commercial PWRs, both soluble boron and control rods are used to start a reactor. In contrast, there is no soluble boron in an SBF system like the ATOM core, so the startup process of the reactor core must be carried out exclusively with the movement of the control rods. In addition, in contrast to the standard PWR startup process, there is no mature experience for the SBF reactor start process. It can be completely different and much faster compared to the standard PWR startup process as it does not need the complicated boration and de-boration process. Additionally, SMRs are said to be more flexible and resilient in terms of power maneuvering compared to commercial large PWRs, and a rapid power ascension is an important design requirement. Therefore, it must be demonstrated that the start of an SBF system from the HZP can be achieved by moving the control rod without any safety problems. Moreover, the start-up process must be examined and

optimized with regard to the power ascension time and the CEA (Control Element Assembly) control logic.

In this paper, a feasibility study for the fast startup of the ATOM core was carried out. For the simulation, the steam generator was decoupled and it was assumed that the inlet coolant temperature has a predetermined value that reflects the change in the demand power. A time-dependent thermal-hydraulics (TH) coupled nodal method was also used for the reactor analysis with the CEA control logic named “Mode-Y” [2].

2. Neutronics Modeling

In this work, the conventional two-step analysis was used to perform the reactor analysis. The burnup-dependent cross-sections, temperature sensitivities, and assembly-wise discontinuity factors (ADFs) were calculated using Serpent-2 3-D Monte Carlo simulations with the ENDF/B-VII.1 cross-section library. The burnup- and temperature-dependent cross-sections were calculated as below:

$$\begin{aligned} & \Sigma_a(Bu, T_f, T_m, D_m) \\ &= \Sigma_a^{ref}(Bu) + \frac{\partial \Sigma_a}{\partial \sqrt{T_f}} \Delta \sqrt{T_f} + \frac{\partial \Sigma_a}{\partial T_m} \Delta T_m \\ &+ \frac{\partial \Sigma_a}{\partial D_m} \Delta D_m + \frac{1}{2} \frac{\partial^2 \Sigma_a}{\partial D_m^2} (\Delta D_m)^2 \\ &+ N_{Hom}^{Xe, \infty}(\phi_g) \sigma_a^{Xe}(Bu, T_f, T_m, D_m) \\ &+ N_{Hom}^{Sm, \infty}(\phi_g) \sigma_a^{Sm}(Bu, T_f, T_m, D_m) \end{aligned} \quad (1)$$

Then, a 3-D nodal analysis was performed with an in-house code, which solves TH-coupled reactor 2-group diffusion equations. The reactor core problem with given conditions was solved with the predictor-corrector quasi-static (PCQS) method based time-dependent nodal expansion method (NEM). Similarly, time-dependent Xe-135 and Sm-149 concentrations were calculated with the following set of equations.

$$N_I(t_n + \Delta t) = N_I(t_n) \quad (2)$$

$$\begin{aligned} & + \Delta t (\gamma_I \sum_{g=1}^G \Sigma_{f,g}(t_n) \phi_g(t_n) - \lambda_I N_I(t_n)) \\ N_{Xe}(t_n + \Delta t) &= N_{Xe}(t_n) + \Delta t (\lambda_I N_I(t_n) + \gamma_{Xe} \sum_{g=1}^G \Sigma_{f,g}(t_n) \phi_g(t_n) \\ & - \lambda_{Xe} N_{Xe}(t_n) - \sum_{g=1}^G \sigma_{Xe,a,g}(t_n) N_{Xe}(t_n) \phi_g(t_n)) \end{aligned} \quad (3)$$

$$\begin{aligned} N_{Pm}(t_n + \Delta t) &= N_{Pm}(t_n) \\ & + \Delta t (\gamma_{Pm} \sum_{g=1}^G \Sigma_{f,g}(t_n) \phi_g(t_n) - \lambda_{Pm} N_{Pm}(t_n)) \end{aligned} \quad (4)$$

$$N_{Sm}(t_n + \Delta t) = N_{Sm}(t_n) + \Delta t(\lambda_{pm} N_{pm}(t_n) - \sum_{g=1}^G \sigma_{Sm,a,g}(t_n) N_{Sm}(t_n) \phi_g(t_n)) \quad (5)$$

The steam generator was decoupled and the coolant inlet temperature was determined by power demand with constant average coolant temperature strategy. It was used because the constant average coolant temperature minimizes the deviation in the primary loop pressure.

3. Thermal-Hydraulic (TH) Modeling

The thermal-hydraulic analysis was carried out for all fuel assemblies in the ATOM core. The information from the reactor analysis is used to calculate axial temperature distributions with given coolant inlet temperature obtained from power demand. In this TH model, the coolant pump was set to 100% power, where the coolant mass flow rate at full power is 2258.78 kg/sec, and both axial heat conduction and lateral momentum were ignored. Therefore, all fuel pin sub-channels have identical TH parameters and all terms related with the lateral momentum are neglected.

First, the axial pressure drop that satisfies the mass balance equation is found from axial momentum balance equation, and the coolant flow velocity and pressure drop are updated until the mass balance is satisfied. Then, the energy balance equation is solved until the enthalpy and coolant temperature converge. Eqs. (6)-(8) are mass balance equation, axial momentum equation, and energy balance equation that are used in TH analysis respectively [3]. Here, the index i stands for axial node level for each assembly channel.

$$(\dot{m}_i - \dot{m}_{i-1}) = -\Delta z_i A_i \frac{\partial \rho_i}{\partial t} \quad (6)$$

$$\frac{(\dot{m}_i v_i - \dot{m}_{i-1} v_{i-1})}{\Delta z_i} + \frac{\partial \dot{m}_i}{\partial t} = -A_i \rho_i g - A_i \frac{\Delta P_i}{\Delta z_i} - \frac{F_i}{\Delta z_i} \quad (7)$$

$$A_i \frac{\partial (\rho_i h_i)}{\partial t} + \frac{(\dot{m}_i h_i - \dot{m}_{i-1} h_{i-1})}{\Delta z_i} = q_i' \quad (8)$$

where,

$$F_i = \frac{1}{2} \left(f \frac{\Delta z \phi^2}{D_h \rho_i} + K V^* \right) \frac{|\dot{m}_i| \dot{m}_i}{A_i}, \quad (9)$$

$$f = a \text{Re}^b, \begin{cases} a = 0.32, b = -0.25 & \text{for laminar} \\ a = 64, b = -1 & \text{for turbulent} \end{cases}$$

$$\text{Re} = \frac{\rho v D_h}{\mu}, \quad D_h = d \left(\frac{4(P/d)^2}{\pi} - 1 \right)$$

In Eq. (7), F_i represents forces from wall friction and form drag. By using Eq. (9), it is calculated with friction factor f , unity phase multiplier ϕ , pressure loss coefficient of grid spacers K , specific volume V^* , and equivalent diameter D_h .

The temperature distribution from the cladding surface to the fuel center is calculated from the

converged axial coolant temperature distribution using finite-difference method (FDM). Eq. (10) briefly describes the system matrix of heat conduction in the fuel and cladding region. The method for creating the system matrix is similar to that of COBRA-III [4]

$$\rho_j C_p V_j \frac{\partial T_j}{\partial t} = Q_j^m V_j + Q_{j-1,j} + Q_{j+1,j}$$

$$Q_{i,j} = K_{i,j} [T_i - T_j],$$

$$K_{i,j} = \frac{2\pi r_i \Delta z (k_i k_j)}{k_j (r_i - \bar{r}_i) + k_i (\bar{r}_j - r_i)}, \quad (10)$$

$$\bar{r}_j = \frac{2(r_j^2 + r_j r_{j-1} + r_{j-1}^2)}{3(r_j + r_{j-1})}$$

where,

$$C_p(T) = \frac{302.27(\theta/T)^2 e^{\theta/T}}{(e^{\theta/T} - 1)^2} + 2 \times 8.463 \times 10^{-3} T + 8.741 \times 10^7 E_a \frac{e^{-E_a/T}}{T^2}, \quad (11)$$

$$T_{fuel,eff} = \frac{23}{25} T_{fuel,average} + \frac{2}{25} T_{fuel,surface} \quad (12)$$

$$k_{fuel} = 1.05 + \frac{2150}{T_{eff} - 73.15}, \quad (13)$$

$$k_{cladding} = 7.51 + 2.09 \times 10^{-2} T_{cl} - 1.45 \times 10^{-5} T_{cl}^2 + 7.67 \times 10^{-9} T_{cl}^3 \quad (14)$$

With Eq. (11), the specific heat capacity of coolant was calculated. Here, θ is Einstein temperature and E_a is the electron activation energy divided by Boltzmann constant [5,6]. The effective fuel temperature for fuel temperature coefficient was calculated using Eq. (12) [7,8]. Then, the thermal conductivities of UO₂ fuel and Zircaloy cladding were determined with Eqs. (13)-(14) [9]. A non-linear iteration was performed until the convergence of temperature, since all TH parameters are temperature-dependent.

4. Numerical Results

In the numerical simulations, the beginning of cycle (BOC) condition was applied to initial power condition, Xe concentration started with equilibrium state, and Sm concentration was set to zero since Sm-149 requires almost infinite time to reach equilibrium at zero power. The demand power rises to 100% after 1 hour, and the total simulation time is set to 30 hours.

In order to simulate the fast startup situation from HZP, the initial control rod positions in the numerical simulations have been set properly: the shutdown bank is all fully withdrawn, mechanical shim banks are fully inserted, and one group of regulating banks is partially withdrawn to reach criticality. The pattern and configuration of various CEAs are shown in Figure 1 [1].

With the beginning of startup process, the CEA control logic Mode-Y determines the withdrawal or insertion of control rods using the temperature difference between the measured coolant outlet temperature and the targeted coolant outlet temperature.

During the transient, 30% overlapping between regulating rods was applied.

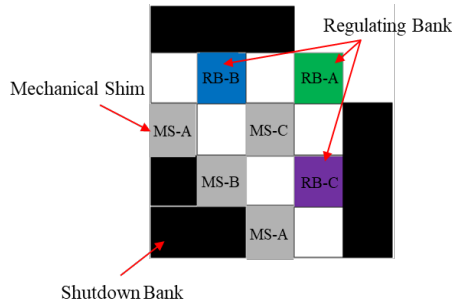


Figure 1. Control Rod Pattern

As seen in Figure 2, the demand power increases rapidly and reaches 100% power at 1 hour. It is shown that the core power well follows the demand without any abnormal behavior.

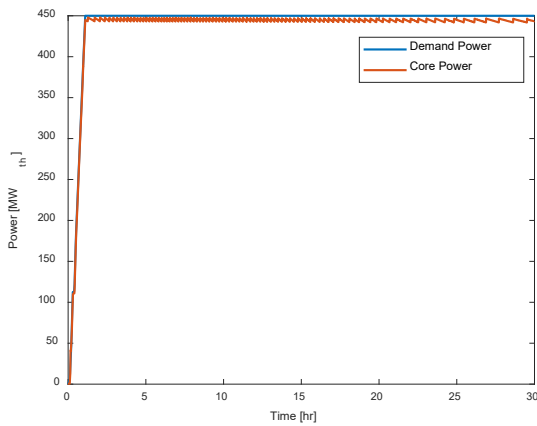


Figure 2. Power Demand

In Figure 3, it is shown that Xe-135 concentration does not oscillate during the transient even with very fast reactor power change. Xe-135 concentration continues to increase after reaching full power due to its long half-life compared with the power ascension rate. Also, Xe-135 is expected to converge after few days as it typically takes about 3 days to reach the equilibrium. In addition, Sm-149 concentration is also still increasing and the convergence will take much longer time because of slow accumulation and lower power density of the ATOM core. This means that the CEAs should be further withdrawn in the future.

The ASI values with given CEA position are plotted in Figure 4. For the general trend, the ASI value initially decreases since RB-C is initially at the upper-half of the core. After the overlapping height, RB-B begins to be withdrawn simultaneously, resulting in an increase in the ASI. Eventually, it decreases with the withdrawal of RB-B and shows increasing behavior again due to the withdrawal of RB-A. This increase is expected to stop soon and the ASI will decrease again when the RB-A is withdrawn beyond the middle point of the active core due to the accumulation of Xe-135 and Sm-149.

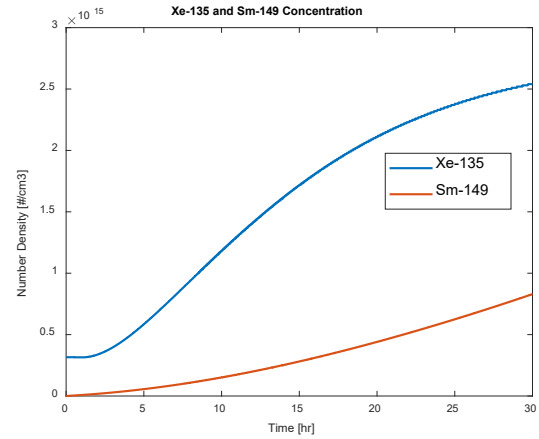


Figure 3. Xe-135, Sm-149 Concentration

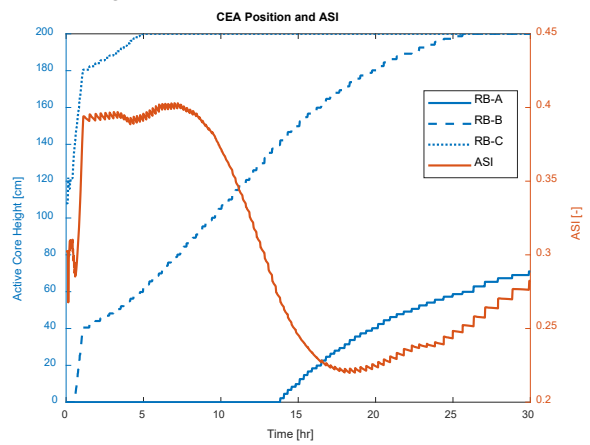


Figure 4. Critical Heights of the various CEAs and ASI

The time-dependent variations of peaking factors and peak heat flux of the core during the startup are shown in Figure 5 and Figure 6. In Figure 5, the 3D peaking factor increases to about 2.2 but it decreases after this global maximum point. The 3D peaking factor is always below 2.35, which is a criterion that could be referred from nuclear design reports. Similarly, in Figure 6, the peak heat flux is always below the limit calculated by multiplying 2.35 to the average heat flux value at the equilibrium state.

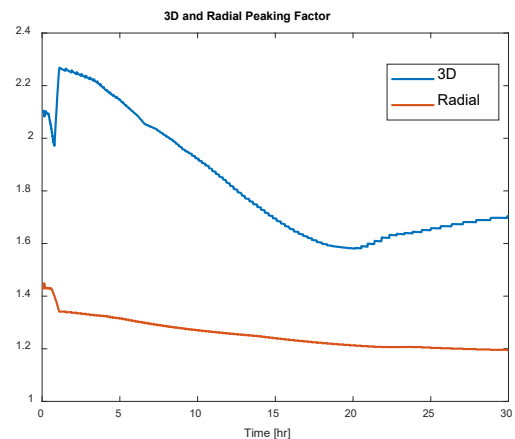


Figure 5. Power peaking factor

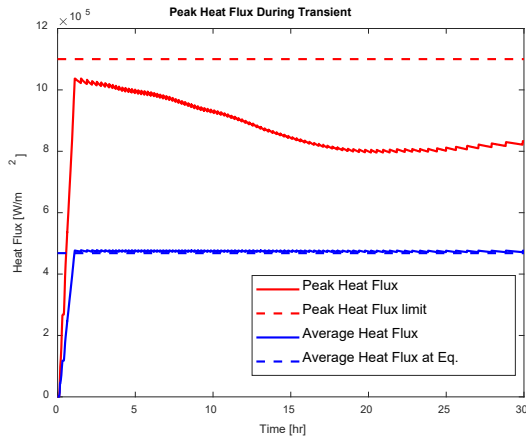


Figure 6. Peak heat flux during transient

Averaged values over the whole fuel assemblies in the ATOM core were used to calculate the inlet and outlet coolant temperature. In Figure 7, the inlet coolant temperature decreased with increasing power demand for the constant average coolant temperature strategy. Moreover, it is shown that the measured outlet coolant temperature is within the temperature dead band ‘0.8K’ during the entire transient by the CEA control logic ‘Mode-Y’.

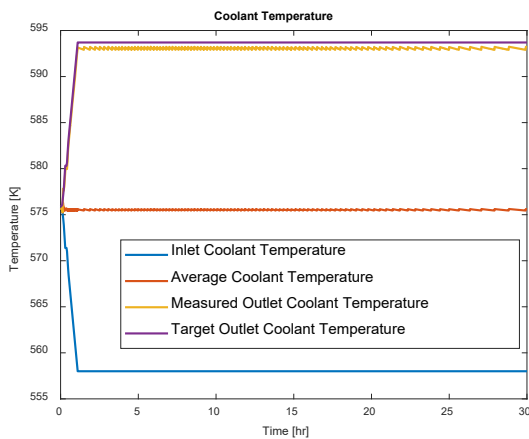


Figure 7. Coolant temperature variation during transient

5. Summary and Conclusions

A time-dependent ATOM core analysis for a reactor startup from hot zero power to hot full power with 3-D TH-coupled PCQS method was performed to validate the feasibility of fast reactor startup in the SBF system. During the transient, CEAs were controlled by the control logic ‘Mode-Y’ with 30% overlapping condition. From the result, the reactor power well followed the demand power even when the power ascension is fast. Also, there was no safety issue in the ASI, peaking factors, and peak heat flux.

Therefore, it was shown that the SBF reactor startup can be done only with automatic control rod movements. For further studies, the in-house code can be optimized for faster calculations. Moreover, the peak heat flux of

fuel rods will be evaluated using reconstructed pin power profile for more accurate evaluation.

ACKNOWLEDGEMENTS

This research was supported by the KAI-NEET, KAIST, Korea and the National Research Foundation of Korea (NRF) Grant funded by the Korean Government (MSIP) (NRF-2016R1A5A1013919).

REFERENCES

- [1] Nguyen, Xuan Ha, ChiHyung Kim, and Yonghee Kim. "An advanced core design for a soluble-boron-free small modular reactor ATOM with centrally-shielded burnable absorber." *Nuclear Engineering and Technology* 51.2 (2019): 369-376.
- [2] Yunseok Jeong, "A Study on Multiphysics Startup simulation of the Soluble-Boron-Free ATOM System", M.S. Thesis, KAIST, 2021
- [3] Chaudri, Khurram Saleem, Jaeha Kim, and Yonghee Kim. "Development and validation of a fast sub-channel code for LWR multi-physics analyses." *Nuclear Engineering and Technology* 51.5 (2019): 1218-1230.
- [4] Basile, D., et al. "COBRA-EN: an upgraded version of the COBRA-3C/MIT code for thermal hydraulic transient analysis of light water reactor fuel assemblies and cores." *Radiation Safety Information Computational Center, Oak Ridge National Lab* (1999).
- [5] Popov, S. G., Juan J. Carbajo, and G. Yoder. "Thermophysical properties of MOX and UO₂ fuels including the effects of irradiation." *ORNL 27* (2000): 4-00.
- [6] Fink, J. K., T. Sofu, and H. Ley. "International nuclear safety center database on thermophysical properties of reactor materials." *International journal of thermophysics* 20.1 (1999): 279-287.
- [7] Grandi, Gerardo, et al. "Effect of CASMO-5 cross-section data and Doppler temperature definitions on LWR reactivity initiated accidents." *Advances in Reactor Physics to Power the Nuclear Renaissance (PHYSOR 2010)* (2010).
- [8] Tomatis, Daniele. "Heat conduction in nuclear fuel by the Kirchoff transformation." *Annals of Nuclear Energy* 57 (2013): 100-105.
- [9] Cho, B., et al. "User's manual for the rectangular three-dimensional diffusion nodal code COREDAX-2 version 1.8." *Korea Advanced Institute of Science and Technology (Aug. 2014)* (2016).